



Gamma dose rate distribution in the Unegt subbasin, a uranium deposit area in Dornogobi Province, southeastern Mongolia

Yasutaka Omori¹ · Atsuyuki Sorimachi¹ · Manlaijav Gun-Aajav² · Nyamdavaa Enkhgerel² · Ganbat Munkherdene² · Galnemekh Oyunbolor² · Amarbileg Shajbalidir³ · Enkhtuya Palam⁴ · Chieri Yamada⁵

Received: 22 April 2019 / Accepted: 3 September 2019 / Published online: 16 September 2019
© Springer-Verlag GmbH Germany, part of Springer Nature 2019

Abstract

Unegt subbasin in Dornogobi Province, southeastern Mongolia, contains the Dulaan Uul uranium deposit, for which development for commercial mining has been conducted as of 2015. Zuunbayan is a commune located close to the Dulaan Uul uranium deposit, and residents of Zuunbayan and their livestock can easily approach the uranium deposit area, including an aboveground dump site, which was created as a result of the mining development. The present study measured and analyzed the gamma dose rate (absorbed dose rate in air) distribution in Unegt subbasin using data collected from a car-borne measurement survey. The gamma dose rate increased from the northern (45–65 nGy/h) to the central (50–69 nGy/h, including Zuunbayan) and the southern (54–195 nGy/h, including Dulaan Uul) parts of the study area. The gamma dose rates (up to 195 nGy/h) around the dump site in Dulaan Uul were significantly higher than the background level (< 80 nGy/h) at several points. Additional in-situ measurements showed that the gamma dose rates reached up to 450 nGy/h at these locations, which was primarily attributed to the gamma radiation emitted by ²³⁸U series elements. Spatial distribution of gamma dose rates around the dump site revealed that the gamma radiation did not originate from the dump, but from the ground, at the measurement points. Analysis of collected soil samples showed that ²³⁸U and ²²⁶Ra were concentrated in deeper soil. These results indicate that the gamma dose rates higher than the background level were not associated with the aboveground mine dump; rather, they were very probably caused by presence of uranium deposits close to the ground surface.

Keywords External exposure · Mining · Potassium · Terrestrial radiation · Thorium · Uranium

Responsible editor: Philippe Garrigues

✉ Yasutaka Omori
ys-omori@fmu.ac.jp

¹ Department of Radiation Physics and Chemistry, Fukushima Medical University, 1 Hikarigaoka, Fukushima 960-1295, Japan

² The Executive Office of the Nuclear Energy Commission, Uildverchid Street 2, Khan Uul District, Ulaanbaatar, Mongolia

³ Center for Hydrology, Meteorology and Environmental Monitoring of Dornogobi Province, Sainshand, Dornogobi, Mongolia

⁴ National Center for Public Health, Ministry of Health, 17 Peace Avenue, Ulaanbaatar, Mongolia

⁵ Department of Public Health Nursing for International Radiation Exposure, Fukushima Medical University, 1 Hikarigaoka, Fukushima 960-1295, Japan

Introduction

The general public is exposed to natural radiation in various ways such as cosmic rays and terrestrial gamma radiation in external radiation exposure and radon inhalation and dietary intake in internal radiation exposure (United Nations Scientific Committee on the Effects of Atomic Radiation 2010). The global annual average dose received from terrestrial gamma radiation, which is the second largest constituent among the natural radiation sources, accounts for one-fifth (0.5 mSv) of the total effective dose (2.4 mSv). Terrestrial gamma radiation is emitted from uranium (²³⁸U) series elements, thorium (²³²Th) series elements, and potassium (⁴⁰K), which are present ubiquitously in the ground. The terrestrial gamma radiation level (i.e., ambient gamma dose rate) depends primarily on the geological setting and soil types constraining the concentrations of these radionuclides (e.g., Quindós et al. 1994; Beamish 2014; Saleh et al. 2015;

Torres et al. 2018). In some cases, however, reported elevations of ambient gamma dose rates were associated with human activities such as mining operations (e.g., Vandenhove et al. 2006; Momčilović et al. 2013; Mangeret et al. 2018).

Mongolia is one of 16 major countries in the world with sizable uranium resources (International Atomic Energy Agency 2018). According to a report on global uranium deposit distribution (International Atomic Energy Agency 2018), the identified recoverable uranium in Mongolia amounted to 141,500 tU (in terms of the weight of uranium metal) in the low-cost category (US\$130/kgU) as of 2014, which accounts for approximately 2% of the global total (7,641,600 tU). In Mongolia, uranium deposits are mostly distributed in the eastern and southeastern parts of the country. According to the International Atomic Energy Agency (2018), of the 21 uranium deposit areas, the Dornod and Dulaan Uul uranium deposits were explored and have been under development for commercial mining as of 2015.

The present study focused on the Unegt subbasin, a part of Dornogobi Province, southeastern Mongolia, which contains the Dulaan Uul uranium deposit (Fig. 1). Based on the presence of radiometric anomalies identified in aerial surveys by scientists of the former Soviet Union in the 1980s, full-fledged exploration for uranium mining started in 1997 in the area. Consequently, a uranium deposit was discovered in 2002 in Dulaan Uul (Cardon et al. 2015; Le Goux et al. 2015; Ariunbileg et al. 2016). The resource amount was estimated as 6,500 tU with an average grade of 0.02% U (Cardon et al. 2015; International Atomic Energy Agency 2018). After the discovery, pilot mining was conducted in 2010 and 2011,

which consisted of uranium extraction by injection of an acid leaching solution into the deposit through wells (Cardon et al. 2015). The uranium deposit area includes the pilot mining site and an aboveground dump site, which came about as a result of the mining development. The area is easily accessible for residents, their livestock, and wildlife such as camels, except for zones marked as restricted during the pilot mining and the dump site.

Only a few radiometric surveys have been conducted in the Unegt subbasin to examine the impact of the presence of uranium deposits on the general public. In 2012, elemental analyses of groundwater were conducted using samples from 202 shallow and deep wells located throughout Dornogobi Province. Severe uranium contamination exceeding the drinking water guideline provided by the World Health Organization was noted in 36% of the samples, mostly from the shallow wells (Nriagu et al. 2013). Ariunbileg et al. (2016) also reported uranium contamination of groundwater sampled from both shallow and deep wells in Dulaan Uul. Distribution of the ambient gamma dose rate is basic information needed for the general public to be aware of the level of radiation to which they are exposed. However, although airborne radiometric surveys were conducted for exploration of uranium deposits (as mentioned previously), the gamma dose rate distribution map is not publicly available at present.

Fukushima Medical University, Japan, and the national and local governments of Mongolia organized a research team to (1) conduct health check examinations and natural radioactivity surveys and (2) introduce a community initiative to respond to radiation exposure for the residents of Zuunbayan,

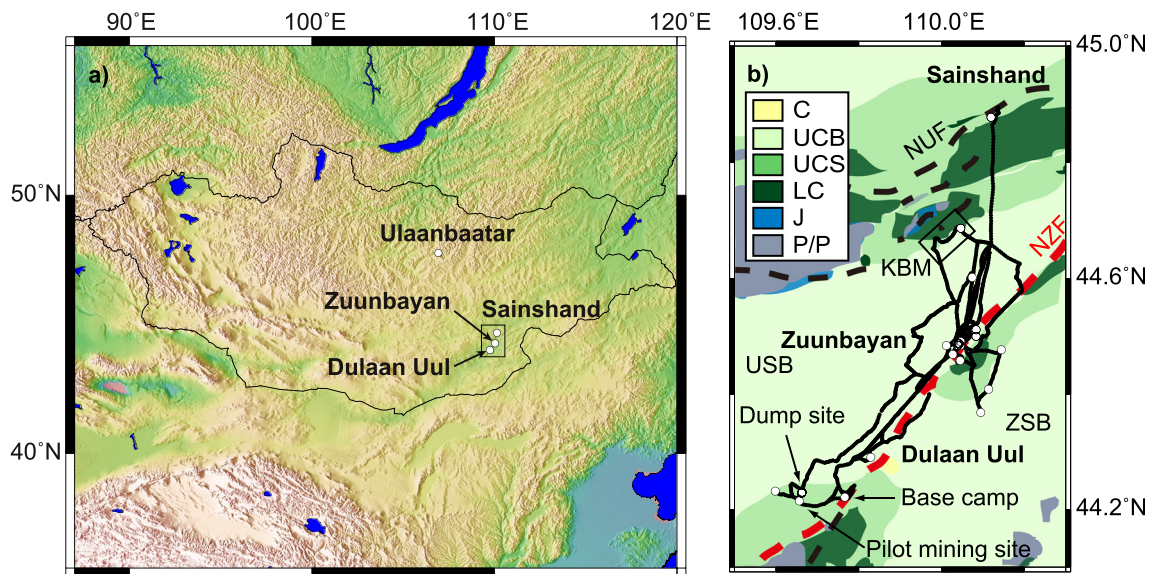


Fig. 1 Location of the study area (a). The survey route is depicted on the geological map (b). In panel b, the open circles represent in-situ measurement and soil sampling locations. P/P, Proterozoic/Paleozoic metamorphic and igneous rocks; J, Jurassic strata; LC, Lower Cretaceous strata; UCS, Upper Cretaceous Sainshand formation; UCB,

Upper Cretaceous Bayanshiree formation; C, Cenozoic strata; NUF, North Unegt fault; NZF, North Zuunbayan fault; USB, Unegt subbasin; ZSB, Zuunbayan subbasin; KBM, Khan Bayanzurkh Mountain. The geological map is based on Grizard et al. (2019) and the topographic data are sourced from Amante and Eakins (2009)

a commune located close to the Dulaan Uul uranium deposits (e.g., Yamada et al. 2018). The natural radioactivity surveys form the focus of the present study, which aims to (1) depict the gamma dose rate distribution in the Unegt subbasin and (2) evaluate the amounts of external and internal radiation exposure from terrestrial gamma radiation and radon in the air for the residents. In the present paper, a gamma dose rate (absorbed dose rate in air) distribution map created using data collected by a car-borne measurement technique is shown. The survey identified gamma dose rates significantly higher than the background level around the dump site. Their origin was discussed based on elemental analyses of the soils.

Materials and methods

Ethics statement

Permissions were obtained from the Ethics Committee of Fukushima Medical University, Japan (No. 2840) and the Nuclear Energy Commission, Government of Mongolia. Consent was also sought from the residents of Zuunbayan when measurements needed to be taken near their dwellings.

Study area

The Unegt subbasin is predominantly located in the central and western parts of Dornogobi Province (Fig. 1). It is oriented toward the northeast, and is 40 km wide and 120 km long (Prost 2004). The northern margin is located near the province's capital, Sainshand, while the eastern margin is bounded by the North Zuunbayan Fault Zone. The basin structure and the accompanying graben and half graben were formed by tectonic extension (rifting) during the Middle Jurassic to Lower Cretaceous (Graham et al. 2001; Prost 2004). Proterozoic to Cenozoic igneous, sedimentary, and metamorphic rocks are distributed in the Unegt subbasin (Fig. 1b; Graham et al. 2001, Cardon et al. 2015; Grizard et al. 2019). Roll-front type uranium mineralization was observed in the Upper Cretaceous Sainshand formation (Cardon et al. 2015; Le Goux et al. 2015). The Sainshand formation is composed of basin-fill deposits, mud-to-conglomerate sequence sediments with disseminated organic matter like lignite deposited in a paleoenvironment consisting of an alluvial fan and a braided plain (Cardon et al. 2015; Le Goux et al. 2015). Given this geological setting, the survey route was planned along the Lower Cretaceous to Upper Cretaceous mud-to-conglomerate sediments, which were partly accompanied by basalt and tuff (Fig. 1b). The study area is characterized by a desert climate and sandy plains and dunes with sparse vegetation.

Zuunbayan and the Dulaan Uul uranium deposits are located close to the eastern margin of the Unegt subbasin (Fig. 1).

The distances between Sainshand and Zuunbayan and between Zuunbayan and Dulaan Uul are approximately 40 km. The population of Zuunbayan is approximately 2,000, and 90% of the residents reside in the commune's center while the other 10% are nomads living around it. Dwellings for the permanent settlers are constructed from mud, bricks, or felt fabric (i.e., yurts), while the nomads only use yurts. Livestock herding is one of the main activities in the area. Dulaan Uul also contains the pilot mining and dump sites as well as a base camp for the mining companies (Fig. 1b). The distance of these sites to the closest dwelling in Zuunbayan was 10–15 km (Fig. 1b) at the time of the survey (July 2017).

Car-borne measurement technique

The car-borne measurement technique was applied to measure the ambient gamma dose rates. It is frequently adopted, instead of walking and airborne measurement techniques, to study the gamma dose rate distribution in a wide area for reasonable spatial resolution and survey period (e.g., Baeza et al. 2013; Hosoda et al. 2015, 2016; Le et al. 2018; Omori et al. 2019). The car-borne technique follows three steps. (1) The rate of gamma radiation (hereafter, count rate) is measured continuously in the moving car. (2) The count rate inside the car is converted to that outside the car to correct for gamma radiation attenuation passing through the car body and its occupants. (3) The corrected count rate is converted into the gamma dose rate. Based on this procedure, the gamma dose rate evaluated in the car-borne measurement technique was formulated as follows:

$$D = N_{in} \times AF \times CF, \quad (1)$$

where D is the absorbed dose rate in air (nGy/h; the gamma dose rate), N_{in} is the count rate (counts/30 s) inside the car, AF is an attenuation factor depending on the car type and number of occupants, and CF is the dose rate conversion factor (nGy/h (counts/30 s)⁻¹), which is used to calculate the absorbed dose rate in air from the corrected count rate (the count rate outside the car).

Count rate inside the car was measured using a 3 in × 3 in cylindrical NaI(Tl) scintillation spectrometer (EMF211, EMF Japan Co., Ltd., Japan) with global positioning system (GPS). It was measured every 30 s along with locality information (latitude and longitude) in the moving car. The car used for the survey was a Russian jeep UAZ-469 with a maximum capacity of five occupants. The spectrometer was set at the center of the backseat of the car (2.5 m from the car bumper, 0.9 m from a side door, and 1.1 m above the ground), and the GPS sensor was placed on the front window inside the car. Three to four occupants were present in the car during the survey. The car speed was 20–50 km/h depending on conditions of the roads,

all of which were sandy except for paved roads in central parts of Sainshand and Zuunbayan.

The attenuation factor was evaluated from the comparison between the count rates inside and outside the car. The count rate outside was the value at 1 m above the sandy ground near the car. These count rates were measured every 30 s for approximately 3 min. Changes in the attenuation factor were also examined in relation to the number of occupants.

The dose rate conversion factor was evaluated from the comparison between the count rates outside the car and the gamma dose rates. In addition to the count rates outside the car, pulse-height distributions of gamma rays at 50–3200 keV were measured for 15 min using the EMF211 at a height of 1 m above the sandy ground. The 22×22 response matrix method (Minato 1978, 2001) was applied to the gamma-ray pulse-height distributions, to unfold them and obtain the incident gamma-ray flux density energy spectra (energy bin widths: 100–280 keV). The absorbed dose rates in air were calculated from the energy and flux densities of the incident gamma rays, mass energy-absorption coefficient for air, and dose conversion factors corresponding to each of the 22 energy bins.

The gamma dose rates calculated from Eq. (1) were mapped through the software Generic Mapping Tools (Wessel et al. 2013) based on the locality information. The relative standard uncertainty of the gamma dose rates involved in count-rate measurement and applications of the attenuation factor and dose rate conversion factor was approximately 10% (coverage factor $k = 2$).

The car-borne survey was conducted from July 4 to 9, 2017, from Sainshand through Zuunbayan to Dulaan Uul. No untoward weather was reported throughout the survey.

In-situ measurement

The incident gamma ray flux density energy spectra were obtained at 31 locations, including those at which the dose rate conversion factor was evaluated, using the method described in the section that deals with the car-borne measurement technique. They were analyzed to determine the contributions of the natural gamma emitter radionuclides present in the ground (^{238}U - and ^{232}Th -series elements and ^{40}K) to the gamma dose rates. The gamma dose rate from each of these radionuclides was determined by focusing on the observed flux density at the photon peaks of ^{40}K (1464 keV), ^{214}Bi (1765 keV and 2205 keV) for the ^{238}U series elements, and ^{208}Tl (2615 keV) for the ^{232}Th series elements (for further details, see Minato (2001) and Omori et al. (2019)). The contribution of radiocesium was ignored in this analysis because its photon peaks were not identified in the gamma-ray pulse-height distributions measured for 15 min. Coefficients of variation depend on the integral absorbed dose in air, and those evaluated by the response matrix method in measurements

repeated 50 times were reported as approximately 2%, 7%, 5%, and 2% for the absorbed dose rates in air from ^{40}K , ^{238}U series elements, ^{232}Th series elements, and the three of them, respectively, at an integral absorbed dose in air of 12 nGy (Matsuda et al. 2002).

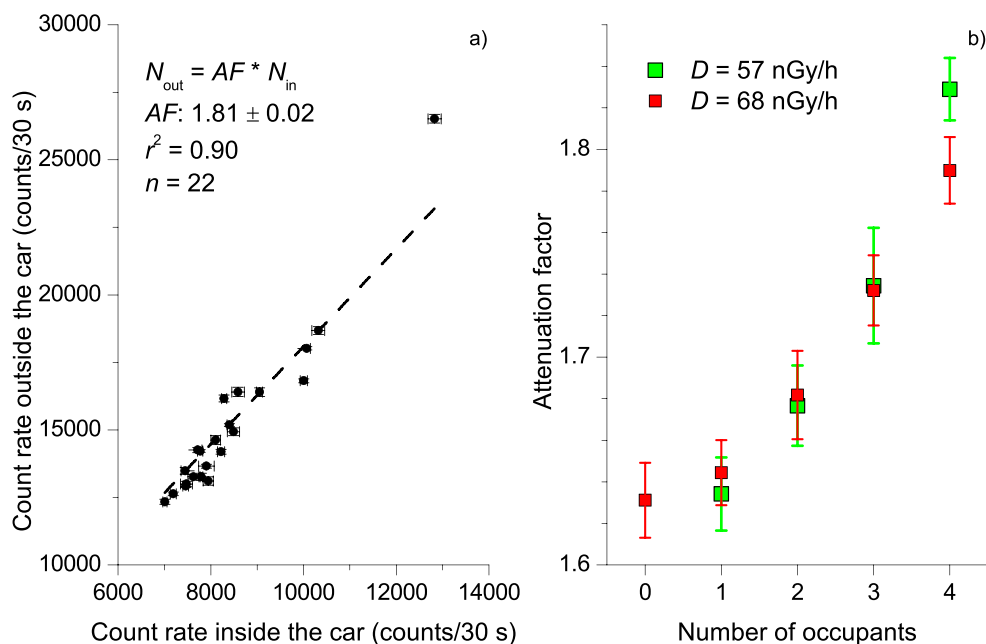
In-situ measurements of gamma dose rates 1 m above ground level were also conducted just along the protective fence surrounding the dump; this was an area that the car could not approach. A CsI(Tl) scintillation survey meter PDR-111 (Hitachi, Ltd., Japan) was used for the measurements. The survey meter displayed an ambient dose equivalent rate (nSv/h), while it was converted into an absorbed dose rate in air after multiplication by a conversion factor of 0.815 Gy/Sv. This conversion factor was obtained from a comparison of the values measured in Zuunbayan (see Fig. 2 in Omori et al. (2019)) using an EMF211 spectrometer and a PDR-111 survey meter. The value of the conversion factor was consistent with a value for environmental gamma radiation according to the International Commission on Radiological Protection (2010). The relative standard uncertainty of the gamma dose rates involved in the measurement of ambient dose equivalent rate and conversion to absorbed dose rate in air was approximately 20% (coverage factor $k = 2$).

Determination of natural radionuclides in the soils of the study area

The soils of the study area were sampled from September 28 to 29, 2018, to determine the activity concentrations of radionuclides, which contributed to the gamma dose rate. In total, 12 soil samples were collected at 8 locations (2 in Sainshand, 2 in Zuunbayan, and 4 in Dulaan Uul). Soils were collected at depths of 0–15 cm at 6 locations, while collections were performed at depths of 0–5 cm, 5–10 cm, and 10–15 cm at the remaining two places (at the dump site in Dulaan Uul). Most terrestrial gamma radiation came from the top 15-cm layer of soil (Kocher and Sjoeren 1985; Yoshioka 1994).

The collected samples were processed at the General Agency for Specialized Inspection, Government of Mongolia. Coarse fractions and impurities were removed using 2-mm mesh size sieves. Then, the samples were dried in an oven at a temperature of 85 °C for 3 h. The dried soil samples, each weighing 750 g, were placed into 500 mL Marinelli beakers and sealed so as to ensure that ^{222}Rn in the ^{238}U decay chain and ^{220}Rn in the ^{232}Th decay chain did not to escape from the beaker. After secular equilibrium was established between the elements of the ^{238}U and ^{232}Th series, gamma spectrometry analysis was performed. A coaxial high purity germanium detector (GC4018, Canberra, USA) with 40% relative efficiency and a resolution of 1.8 keV (FWHM) at 1330 keV was used for the analysis. Detector energy calibration and absolute photon peak efficiency were estimated using LabSOCS/ISOCS Calibration Software based

Fig. 2 Correlation between count rates inside and outside the car (a) and attenuation factors with respect to the number of occupants in the car (b)



on 3D Geometry Composer. To determine the activity concentrations, gamma lines at 1001 keV of $^{234\text{m}}\text{Pa}$ for ^{238}U , 609 and 1120 keV of ^{214}Bi and 295 and 352 keV of ^{214}Pb for ^{226}Ra , 338 and 911 keV of ^{228}Ac and 239 keV of ^{212}Pb for ^{232}Th , and 1461 keV of ^{40}K were used. The measurement time was 1 h. The minimum detectable activity concentrations of ^{40}K , ^{238}U , ^{226}Ra , and ^{232}Th were 30 Bq/kg, 60 Bq/kg, 5 Bq/kg, and 4 Bq/kg, respectively. The relative standard uncertainties of the activity concentrations involved in the stable operation of gamma spectrometry, statistical error of the analysis and uncertainties for weight gauge, processed volume, and detector efficiency were 7% for ^{40}K , 11–25% for ^{238}U , 7–14% for ^{226}Ra , and 9–18% for ^{232}Th (coverage factor $k = 2$).

Results and discussion

Attenuation factor and dose rate conversion factor

Figure 2a shows scatter plot of the count rates outside the car against those inside it with four occupants. The count rates were measured at 22 fixed points for gamma dose rates of 48–90 nGy/h. A linear relationship with a high determination coefficient (0.90) was found between them. The slope of the regression line passing through the origin was calculated to be 1.81 (standard error 0.02). An experiment was also conducted at 2 of the 22 fixed points (at 57 nGy/h and 68 nGy/h) to examine the effect of the number of occupants on the attenuation factor. In this experiment, the attenuation factor was the count rate ratio in a pair of inside and outside measurements. Figure 2b presents the scatter plot of the attenuation factors against the number of

occupants in the car. The results showed that the attenuation factor increased with the number of occupants. The attenuation factors of the car body itself and the car including four occupants were approximately 1.63 and 1.81, respectively, and their difference was 10%. This finding indicates that the car body plays a primary role, but the number of occupants also slightly influences the attenuation factor. For four occupants, the attenuation factor in Fig. 2b was consistent with that in Fig. 2a. In the present study, the attenuation factors of 1.73 and 1.81 were considered as AF in Eq. (1) when the number of occupants was three and four, respectively. These values showed good agreement with the range of 1.47–1.80 obtained using a similar method for studies conducted in other countries (Baeza et al. 2013; Hosoda et al. 2015, 2016; Le et al. 2018; Omori et al. 2019), although a strict comparison could not be made due to the differences in car types and the number of occupants.

Figure 3 shows a scatter plot of the gamma dose rates against the count rates outside the car. The measurements were made at 26 fixed points where the gamma dose rates ranged from 48–295 nGy/h. A linear relationship with a high determination coefficient (0.98) was found between them. The slope of the regression line passing through the origin was calculated to be 4.00×10^{-3} nGy/h (counts/30 s) $^{-1}$ (standard error 0.06×10^{-3} nGy/h (counts/30 s) $^{-1}$). Thus, the dose rate conversion factor of 4.00×10^{-3} nGy/h (counts/30 s) $^{-1}$ was substituted for CF in Eq. (1) in the present study. This value agreed well with the range of 3.8×10^{-3} – 5.2×10^{-3} nGy/h (counts/30 s) $^{-1}$ reported by Hosoda et al. (2015, 2016) and Le et al. (2018). Omori et al. (2019) also calculated absorbed dose rates in air along Asian Highway 3 in Mongolia based on the relationship in Fig. 3.

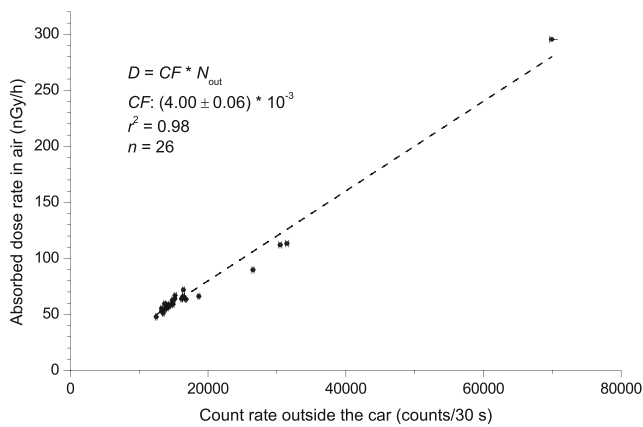


Fig. 3 Correlation between gamma dose rates and count rates outside the car. This figure was reproduced from Omori et al. (2019) with permission from Oxford University Press

Gamma dose rate distribution in the Unegt subbasin

Figure 4 presents the gamma dose rate distribution map obtained using the car-borne survey in the study area. The gamma dose rates ranged from 45 to 195 nGy/h. The lowest gamma dose rate was obtained at Mt. Khan Bayanzurkh, while the highest was observed at the dump site in Dulaan Uul (details of the survey at the dump site are presented in the next section). Figure 5 presents cumulative frequency distributions of the gamma dose rates in the northern, central, and southern parts of the study area, which include Sainshand, Zuunbayan, and Dulaan Uul, respectively. The location of each area is depicted in Fig. 4. The cumulative frequency distributions show clear differences in the gamma dose rate among the three areas. The gamma dose rates were higher in the southern part compared to those in the northern and central parts. The average gamma dose rates were 56 nGy/h (range 45–65 nGy/h) in the northern part, 58 nGy/h (range 50–69 nGy/h) in the central part, and 67 nGy/h (range 54–195 nGy/h) in the southern part.

The gamma dose rates were summarized with respect to landmarks in the study area: the communes of Sainshand and Zuunbayan, Mt. Khan Bayanzurkh, oil fields, wells, water ponds in Zuunbayan and Dulaan Uul, the pilot mining site, and the dump site. Statistical values [average ± standard deviation (range; number of data points)] were 60 ± 3 nGy/h (56–65 nGy/h; n = 15) at Sainshand, 57 ± 2 nGy/h (50–68 nGy/h; n = 247) at Zuunbayan, 51 ± 3 nGy/h (45–57 nGy/h; n = 57) at Mt. Khan Bayanzurkh, 61 ± 5 nGy/h (52–69 nGy/h; n = 47) at oil fields, 56 ± 6 nGy/h (45–61 nGy/h; n = 12) at wells, 57 ± 3 nGy/h (51–69 nGy/h; n = 56) at water ponds, 64 ± 1 nGy/h (63–65 nGy/h; n = 5) at the pilot mining site, and 90 ± 27 nGy/h (62–195 nGy/h; n = 74) at the dump site. Compared to the gamma dose rates at the dump site, these values were lower and similar to those at the other sites, including the pilot mining site.

Table 1 presents the contributions of the ²³⁸U and ²³²Th series elements as well as ⁴⁰K to the gamma dose rates at 31

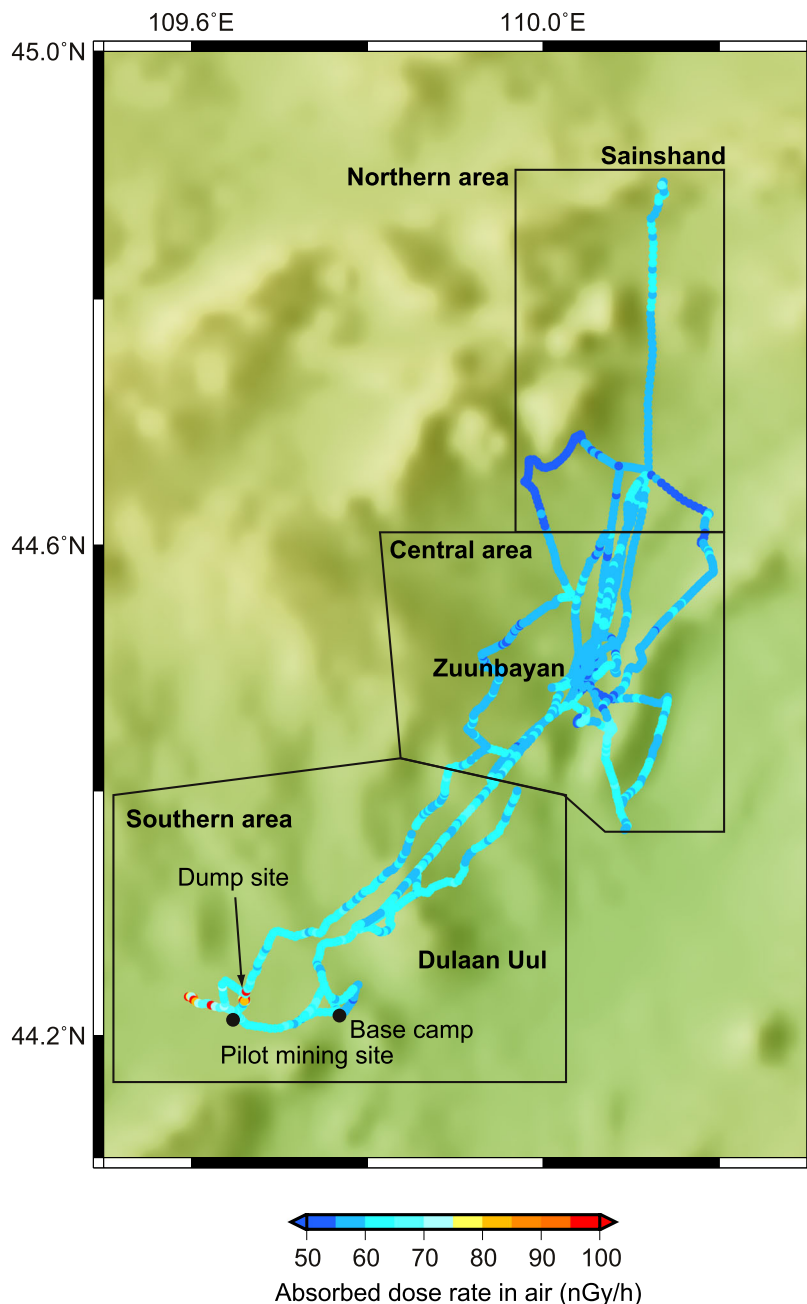
fixed points. The gamma dose rates from the ²³²Th series elements and ⁴⁰K ranged from 10 to 25 nGy/h and 24–37 nGy/h, respectively, which appeared to be constant throughout the areas. In contrast, the gamma dose rates from the ²³⁸U series elements tended to be constant (9–23 nGy/h) in the northern and central parts, while they varied (15–401 nGy/h) in the southern part, especially at the dump site. This finding indicates that the greater abundance of the ²³⁸U series elements in the soil caused the higher gamma dose rates in the southern part.

Gamma dose rate anomaly around the dump site in Dulaan Uul

The high gamma dose rates were not distributed homogeneously. Rather, they appeared in patches, like “hot spots”, around the dump site. Figure 6a presents a detailed map of the gamma dose rate around that site. The map was created using data from the car-borne measurement technique in which the car speed (4–8 km/h) was as low as possible because the site was not very large (240 m × 130 m). The results showed high gamma dose rates (80–195 nGy/h) concentrated in a specific area, which was oriented northeast-southwest and measured approximately 320 m in length and 250 m in width. The distribution direction was consistent with both the uranium roll-front distribution direction in Dulaan Uul (Cardon et al. 2015) and the annual wind direction observed at the Center for Hydrology, Meteorology, and Environmental Monitoring of Dornogobi Province located at Sainshand. For the other points, the gamma dose rates ranged from 62 to 79 nGy/h. This range showed fairly good agreement with the values noted in the northern and central parts of the study area (45–69 nGy/h); therefore, the gamma dose rates at these points can be regarded as the background level. In contrast, the gamma dose rates obtained from the in-situ measurements using the spectrometer and survey meter were 65–450 nGy/h (Fig. 6b and Table 1). The gamma dose rates that were higher than the background level and were measured using the car-borne technique tended to be lower than those obtained using the in-situ measurements. This tendency confirms that the points with high gamma dose rate points were only localized; they could be considered as hot spots.

The in-situ measurements were also made to clarify the constitutional difference in the gamma dose rates between the points displaying high dose rates (n = 4) and background dose rate (n = 2). As presented in Table 1, very minor differences in the gamma dose rates from the ²³²Th series elements and ⁴⁰K were found between the points displaying the high dose rates (²³²Th, 15–17 nGy/h; ⁴⁰K, 30–32 nGy/h) and those displaying background dose rates (²³²Th, 17 nGy/h; ⁴⁰K, 28 nGy/h and 31 nGy/h). However, clear difference was found in the gamma dose rates from the ²³⁸U series elements (points showing high dose rates: 65–401 nGy/h; points

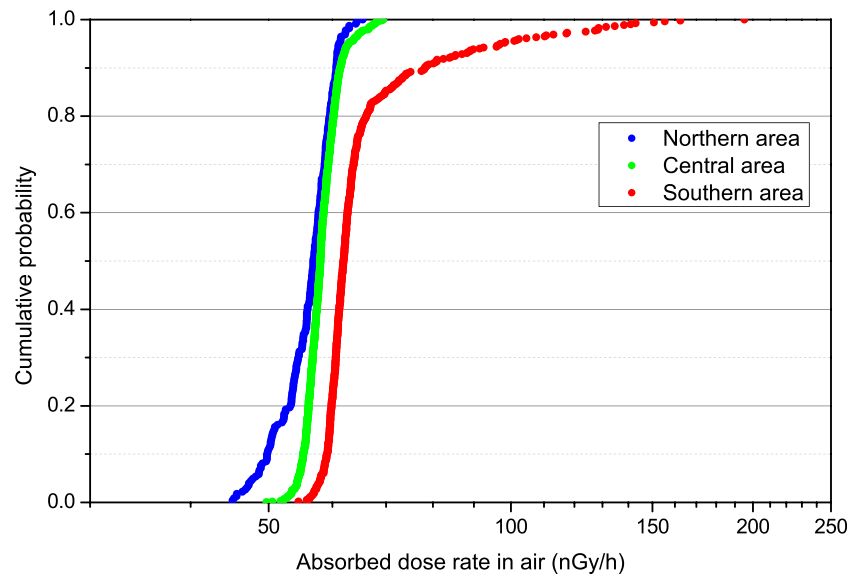
Fig. 4 Gamma dose rate distribution map of the study area



showing background dose rates: 21 nGy/h and 22 nGy/h). As per Fig. 6 and Table 1, the gamma dose rates were independent of the distance from the dump (or the protective fence). In fact, the maximum gamma dose rate (450 nGy/h) was obtained at a point located 50 m from the protective fence (point 30 in Table 1). In addition, at one point displaying a high dose rate, the gamma dose rate at 0.1 m height was 1.5 times higher than that at 1.0 m height (point 28 in Table 1). These findings indicate that the source of the ^{238}U series elements contributing to the high gamma dose rates is concentrated in the ground at the measurement points rather than within the dump.

Soils around the dump site were sampled at 0–15 cm depths to determine the concentrations of natural radionuclides (^{238}U , ^{226}Ra , ^{232}Th , and ^{40}K elements). At the points showing high gamma dose rates, the soils at three depth intervals (0–5 cm, 5–10 cm, and 10–15 cm) were analyzed to investigate the depth profiles of the radionuclide concentrations. For comparison, soils in the northern and central parts of the study area were also sampled. Table 2 presents the activity concentrations of the ^{238}U , ^{226}Ra , ^{232}Th , and ^{40}K elements at eight points, among which two were sampled to be high-dose-rate points (these were same as points 28 and 30 in Table 1). Similar to fractional distributions of each gamma dose rate

Fig. 5 Cumulative frequency distributions of gamma dose rates in the northern, central, and southern parts of the study area. The location of each part is depicted in Fig. 4



from the natural radionuclides in Table 1, no clear areal differences in the activity concentrations were found for ^{232}Th (18–42 Bq/kg) and ^{40}K (730–1028 Bq/kg) throughout the study area. These concentrations were relatively higher than those (^{232}Th , 13–16 Bq/kg; ^{40}K , 420–650 Bq/kg) for three Mongolian soil samples collected throughout the country (Tserenpil et al. 2013). ^{232}Th concentrations were also close to the global average of 45 Bq/kg, while ^{40}K concentrations were higher than the global average of 420 Bq/kg (United Nations Scientific Committee on the Effects of Atomic Radiation 2010).

Unlike the ^{232}Th and ^{40}K concentration, unusual contrasts in ^{238}U and ^{226}Ra concentrations were found in the study area. The ^{226}Ra concentrations could be evaluated for all the samples, and they were 19–30 Bq/kg in the northern and central areas and 26–3630 Bq/kg in the southern area. The ^{238}U concentrations (100–1220 Bq/kg) for the soil samples could only be successfully evaluated only at two points that showed high dose rates due to the high minimum detectable activity concentration (60 Bq/kg) of the adopted gamma-spectrometry system. The ^{238}U and ^{226}Ra concentrations around the dump site were two orders of magnitude higher than those (^{226}Ra , 10–22 Bq/kg) for the Mongolian soils (Tserenpil et al. 2013) and the global average of 33 Bq/kg (^{238}U) and 32 Bq/kg (^{226}Ra) (United Nations Scientific Committee on the Effects of Atomic Radiation 2010). The depth profiles at these points shared a certain trend, namely that the ^{238}U and ^{226}Ra were concentrated in the deeper soil. At the point displaying the highest dose rate, the ^{238}U and ^{226}Ra concentrations at 10–15 cm in depth were approximately 3 times higher than those at 0–5 cm. These findings mean that the ^{238}U series elements contributing to the high gamma dose rates are located within deeper soils rather than at the ground surface.

What constrains gamma dose rate distribution?

A series of measurements confirm that the high gamma dose rates were not of artificial origin; they could not be attributed to the existence of the dump site. Regarding the origin, the first hypothesis was that the gamma rays originated directly from the dump. However, this was rejected because of results that showed that the variation in the gamma dose rate was independent of the distance from the dump and that the ^{238}U source was located at the measurement points. The second hypothesis was that the ^{238}U series elements were discharged from the dump and that their influence extended beyond the protective fence due to meteorological erosion caused by strong winds and heavy rainfall. This hypothesis seemed unlikely as the results showed that the ^{238}U and ^{226}Ra elements were not concentrated in the surface soil. Another hypothesis was that ^{238}U mineralized naturally, close to the surface of the ground. In such a case, the depth should extend up to several tens of centimeters, considering the self-adsorption of gamma rays in the soil. Uranium deposit outcrops are considered to be a natural phenomenon; they have been frequently reported around the world (e.g., War et al. 2008; Bollhöfer et al. 2014; Akata et al. 2017). In Dulaan Uul, uranium deposits are enclosed in sandstone beds of the Upper Cretaceous Sainshand formation. Thus, they appear between oxidized and reduced sands, and mineralization occurred at depths ranging from a few meters to 300 m (Cardon et al. 2015). In the present study, anomalies in the gamma dose rate were observed at locations where the Upper Cretaceous Sainshand formation was exposed. In addition, the locations and the distribution direction of the high-gamma-dose-rate points were consistent with those of the uranium roll-front reported by Cardon et al. (2015). Some of the uranium deposits may be located at the ground surface. This possibility was supported by the depth profiles of ^{238}U and the

Table 1 Gamma dose rates and contributions of ^{40}K , ^{238}U , and ^{232}Th to gamma dose rates

| Location | | | | Gamma dose rate (nGy/h) | | | | Contribution (%) | | | Remarks |
|----------|----------|---------------------------------|----------------------------------|-------------------------|-----------------|------------------|-------------------|------------------|------------------|-------------------|--|
| Code | Area | Latitude ($^{\circ}\text{N}$) | Longitude ($^{\circ}\text{E}$) | Total | ^{40}K | ^{238}U | ^{232}Th | ^{40}K | ^{238}U | ^{232}Th | |
| 1 | Northern | 44.8778 | 110.1179 | 61 | 32 | 15 | 14 | 53 | 24 | 23 | Center of Sainshand |
| 2 | | 44.6869 | 110.0449 | 82 | 34 | 23 | 25 | 42 | 28 | 30 | Mt. Khan Bayanzurkh |
| 3 | Central | 44.4691 | 110.0255 | 66 | 31 | 14 | 21 | 46 | 22 | 32 | Center of Zuunbayan |
| 4 | | 44.4844 | 110.0100 | 64 | 32 | 13 | 18 | 51 | 21 | 29 | Center of Zuunbayan |
| 5 | | 44.4844 | 110.0436 | 58 | 30 | 14 | 14 | 51 | 25 | 24 | Center of Zuunbayan |
| 6 | | 44.4913 | 110.0445 | 63 | 30 | 19 | 13 | 48 | 31 | 21 | Center of Zuunbayan |
| 7 | | 44.4871 | 110.0389 | 55 | 34 | 10 | 12 | 61 | 18 | 21 | Center of Zuunbayan |
| 8 | | 44.4878 | 110.0367 | 59 | 31 | 16 | 12 | 53 | 27 | 20 | Center of Zuunbayan |
| 9 | | 44.4875 | 110.0411 | 67 | 34 | 16 | 17 | 50 | 25 | 25 | Center of Zuunbayan |
| 10 | | 44.4872 | 110.0411 | 72 | 34 | 18 | 19 | 48 | 26 | 27 | Center of Zuunbayan |
| 11 | | 44.4845 | 110.0378 | 55 | 29 | 12 | 14 | 52 | 22 | 25 | Center of Zuunbayan |
| 12 | | 44.4844 | 110.0378 | 55 | 28 | 12 | 15 | 51 | 21 | 28 | Center of Zuunbayan |
| 13 | | 44.4886 | 110.0388 | 62 | 37 | 12 | 13 | 60 | 20 | 20 | Center of Zuunbayan |
| 14 | | 44.4771 | 110.1427 | 59 | 31 | 12 | 15 | 54 | 20 | 26 | |
| 15 | | 44.3685 | 110.0929 | 56 | 31 | 12 | 13 | 55 | 22 | 23 | |
| 16 | | 44.5117 | 110.0818 | 51 | 29 | 12 | 10 | 56 | 24 | 20 | Well |
| 17 | | 44.4089 | 110.1122 | 57 | 32 | 14 | 11 | 55 | 25 | 20 | Well |
| 18 | | 44.5004 | 110.0820 | 53 | 30 | 12 | 11 | 57 | 23 | 20 | Water place |
| 19 | | 44.5001 | 110.0815 | 59 | 29 | 15 | 14 | 49 | 26 | 25 | Water place |
| 20 | | 44.4584 | 110.0433 | 48 | 29 | 9 | 10 | 60 | 19 | 21 | Water place |
| 21 | | 44.6021 | 110.0725 | 59 | 24 | 15 | 20 | 41 | 26 | 33 | |
| 22 | Southern | 44.2908 | 109.8273 | 64 | 30 | 18 | 16 | 47 | 28 | 25 | Dwelling closest to Dulaan Uul |
| 23 | | 44.2216 | 109.7649 | 61 | 28 | 15 | 17 | 46 | 25 | 29 | Base camp |
| 24 | | 44.2149 | 109.6549 | 64 | 27 | 21 | 16 | 42 | 34 | 25 | Pilot mining site |
| 25 | | 44.2287 | 109.6608 | 66 | 28 | 22 | 17 | 42 | 33 | 25 | Dump site |
| 26 | | 44.2284 | 109.6603 | 69 | 31 | 21 | 17 | 46 | 30 | 24 | Dump site |
| 27 | | 44.2300 | 109.6612 | 112 | 30 | 67 | 15 | 27 | 59 | 14 | Dump site; Distance from fence 0.6 m |
| 28-1 | | 44.2300 | 109.6612 | 295 | 32 | 247 | 16 | 11 | 84 | 5 | Dump site; Distance from fence 7 m; Height 1 m |
| 28-2 | | 44.2300 | 109.6612 | 444 | 33 | 393 | 17 | 8 | 89 | 4 | Dump site; Distance from fence 7 m; Height 0.1 m |
| 29 | | 44.2300 | 109.6614 | 113 | 31 | 65 | 17 | 27 | 58 | 15 | Dump site; Distance from fence 15 m |
| 30 | | 44.2306 | 109.6616 | 450 | 32 | 401 | 17 | 7 | 89 | 4 | Dump site; Distance from fence 50 m |
| 31 | | 44.2321 | 109.5967 | 90 | 24 | 48 | 17 | 27 | 54 | 19 | Black shale |

maximum concentration of 1220 Bq/kg, two orders of magnitude higher than the global average. Given the present status, this hypothesis cannot be rejected.

The collected soil samples in the present study presented high $^{226}\text{Ra}/^{238}\text{U}$ activity ratios (4–13 ($20 <$)) that far exceeded unity (i.e., large disequilibrium between these two elements). However, this finding does not necessarily mean that the uranium-depleted soils contained residual solids discharged

from uranium mining activity. High $^{226}\text{Ra}/^{238}\text{U}$ ratios (on the order of 10) have been reported for natural soil (rock) samples in some studies (e.g., Levinson and Bland 1978; Von Gunten et al. 1996; Dowdall and O’Dea 2002; Boulesteix et al. 2019). These were attributed to the enrichment of radium by sorption onto soil particles and depletion of uranium by dissolution in soil water followed by migration to other locations (Von Gunten et al. 1996; Dowdall and O’Dea

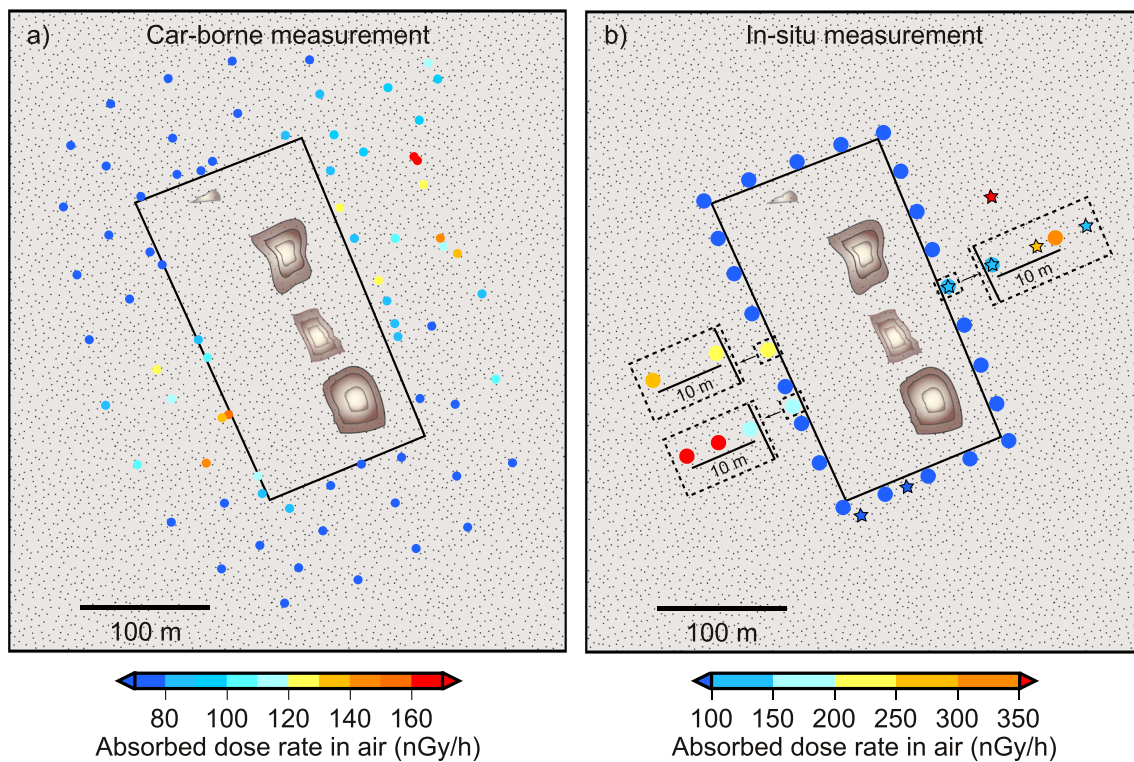


Fig. 6 Gamma dose rate distribution around the dump site, using data collected from the car-borne measurement (a) and in-situ measurements (b). In panel b, the stars and circles represent gamma dose rates measured using the spectrometer and survey meter, respectively

2002). In particular, for the case of the roll-front type uranium deposits in Kazakhstan reported by Boulesteix et al. (2019), $^{226}\text{Ra}/^{238}\text{U}$ ratios exceeding 10 were observed in the upstream portion (oxidized zones) of the orebody, in which uranium was oxidized to soluble uranium forms while radium was immobile. Although the origin of the high $^{226}\text{Ra}/^{238}\text{U}$ ratios in the present study is not confirmed, the ratios are not necessarily related to uranium mining activity.

Based on the above discussion, this study indicates that gamma dose rates higher than the background level were not associated with the aboveground mining dump, but were most probably caused by a uranium deposit located close to the ground surface.

Background gamma dose rates obtained in the car-borne surveys were slightly higher in the southern area than those in the other areas (Figs. 4 and 5). This characteristic was not determined from the in-situ measurements (Tables 1 and 2), possibly due to the small number of measurement points. In general, the gamma dose rate depends primarily on whether the soil composition includes the natural radionuclides. However, in the present study, the cause of the areal difference is not presently clear, because there seems to be a poor relationship between gamma dose rate distribution and surface geology (Figs. 1b and 4). One potential reason is that lithofacies differ even within the same strata. It may be caused by varying deposition paleoenvironments. For the case of the Upper Cretaceous Sainshand formation, silicic clasts were

discharged from the northern basin boundary, and they formed an alluvial fan and a braided plain from north to south (Le Goux et al. 2015). Another potential reason for the observed gamma dose rate distribution is the dense surface fractures in the southern area. According to the geological map given in Cardon et al. (2015) and Le Goux et al. (2015), minor faults, which are related to graben and half-graben basin structure (not depicted in Fig. 1b), are densely distributed in the southern area. Torres et al. (2018) reported that the gamma dose rate distribution was partly constrained by the presence of faults. Detailed surveys are required to clarify the cause of the areal difference.

Impact on the public residing in the vicinity of the study area

In the present survey, the measured gamma dose rates were 45–195 nGy/h as per car-borne measurements and 48–450 nGy/h according to the in-situ measurements. Of all the measurement points, 97% had a gamma dose rate of less than 80 nGy/h, which was regarded as the background level. According to Omori et al. (2019), the gamma dose rates ranged from 50 to 90 nGy/h along Asian Highway 3 between Ulaanbaatar and Sainshand. United Nations Scientific Committee on the Effects of Atomic Radiation (2010) estimated that 86% of inhabitants in the world are exposed to terrestrial radiation up to 80 nGy/h. Throughout most of the study

Table 2 Activity concentrations of ^{238}U , ^{226}Ra , ^{232}Th , and ^{40}K

| Location | | | | Concentration ^a (Bq/kg) | | | | Remarks |
|----------|----------|---------------|----------------|------------------------------------|------------------|-------------------|-------------------|----------------------------|
| Code | Area | Latitude (°N) | Longitude (°E) | ^{40}K | ^{238}U | ^{226}Ra | ^{232}Th | |
| 1 | Northern | 44.8778 | 110.1179 | 730 ± 52 | < 60 | 28 ± 3 | 28 ± 3 | #1 ^b |
| 2 | | 44.6869 | 110.0449 | 1028 ± 72 | < 60 | 30 ± 3 | 40 ± 4 | #2 ^b |
| 3 | Central | 44.4886 | 110.0388 | 966 ± 68 | < 60 | 20 ± 2 | 18 ± 2 | #13 ^b |
| 4 | | 44.5117 | 110.0818 | 915 ± 64 | < 60 | 19 ± 2 | 18 ± 2 | #16 ^b |
| 5 | Southern | 44.2908 | 109.8273 | 905 ± 63 | < 60 | 43 ± 6 | 26 ± 3 | #22 ^b |
| 6 | | 44.2284 | 109.6603 | 995 ± 70 | < 60 | 26 ± 3 | 34 ± 3 | #26 ^b |
| 7-1 | | 44.2300 | 109.6612 | 851 ± 58 | < 60 | 1257 ± 87 | 36 ± 5 | #28 ^b 0–5 cm |
| 7-2 | | | | 883 ± 63 | < 60 | 1242 ± 109 | 38 ± 5 | 5–10 cm |
| 7-3 | | | | 914 ± 63 | 100 ± 25 | 1276 ± 88 | 35 ± 5 | 10–15 cm |
| | | | | 883 | - | 1258 | 36 | 0–15 cm ^c |
| 8-1 | | 44.2306 | 109.6616 | 866 ± 63 | 450 ± 50 | 1876 ± 164 | 42 ± 6 | #30 ^b 0–5 cm |
| 8-2 | | | | 827 ± 62 | 960 ± 120 | 3682 ± 321 | 38 ± 7 | 5–10 cm |
| 8-3 | | | | 815 ± 61 | 1220 ± 150 | 5332 ± 465 | 46 ± 8 | 10–15 cm |
| | | | | 836 | 877 | 3630 | 42 | 0–15 cm ^c |

^a Minimum detectable activities (MDAs) were 30 Bq/kg for ^{40}K , 60 Bq/kg for ^{238}U , 5 Bq/kg for ^{226}Ra , and 4 Bq/kg for ^{232}Th

^b The location appears in Table 1

^c The concentrations were averaged at three depth intervals

area, the gamma dose rates are comparable to those observed in the rest of the world.

On the other hand, the gamma dose rates higher than 80 nGy/h and up to 450 nGy/h were obtained at 3% of the measurement points. Based on the maximum value, the most conservative evaluation of annual effective dose did not exceed 2.3 mSv/y (this value excludes the background dose of 0.5 mSv/y). The evaluated value was higher than the lower bound of the reference level range (1–20 mSv/y) in existing exposure situations for naturally occurring radioactive materials, natural radiation, and radioactive residues in the living environment, as recommended by the International Commission on Radiological Protection (International Commission on Radiological Protection 2007). However, as shown in Fig. 6 and Table 1, the points with high gamma dose rates are distributed patchily. In addition, these gamma dose rates are not as high compared to those in high background radiation areas such as Kerala (India) and Yangjiang (China). The measured gamma dose rates ranged from 40 to 2100 nGy/h outdoors in Kerala (Hosoda et al. 2015) and 260–600 nGy/h indoors in Yangjiang (Morishima et al. 2000). No health effects due to external radiation exposure were observed from epidemiological studies in these areas (e.g., Nair et al. 2009; Tao et al. 2012). Thus, no health effects due to chronic external exposure to terrestrial radiation are expected in the areas surveyed in the present study.

Unintended inhalation and dietary intake of uranium and radium may pose some health risk. The present study revealed that a part of the uranium deposits are probably present close to the ground surface. Thus, these deposits can be easily accessible for the residents and animals, including their livestock. Generally, subsurface soil exists under oxic conditions, under which uranium tends to dissolve into water. Thus, it is possible that the dissolved uranium can leach into soil moisture, surface water, and aquifers and be taken up by plants (including crops), animals, and finally, the residents. Ariunbileg et al. (2016) reported a high uranium contamination in shallow and deep well water, exceeding the guideline level for drinking water in Dulaan Uul. Unlike uranium, radium tends to be immobile in the surficial soil layer (Dowdall and O'Dea 2002; Vandenhove et al. 2010). This is implied by the high $^{226}\text{Ra}/^{238}\text{U}$ activity ratios in the soil samples collected in the present study. However, it has been found that plants can take up radium from the soil (Vandenhove et al. 2010). Moreover, studies have found that the amount of radium taken up by plants from the soil is more than that of uranium (Greeman et al. 1999). Both the previous and present studies did not investigate the uranium and radium content in suspended particles in the air and foodstuffs. These measurements would be required to fully understand the health effects of uranium series elements on the residents in the study area.

Conclusions

The Unegt subbasin in Dornogobi Province, southeastern Mongolia, contains uranium deposits. The uranium mining sites are located in close vicinity to a residential area. To understand the possible health risk posed by the mining to these residents and their livestock, the gamma dose rates in the study area were obtained using the car-borne technique and in-situ measurements. The measured values were 45–195 nGy/h and 48–450 nGy/h, respectively. The locations with high gamma dose rates were situated around the aboveground mine dump and were distributed patchily, akin to hot spots, which indicated points at which ^{238}U and ^{226}Ra were concentrated deeper in the soil. Additional investigations revealed that these high dose rates could not be attributed to the mining activities; rather, they probably indicated the presence of uranium deposits close to the ground surface. The gamma dose rates indicated no possibility of adverse health effects due to chronic external exposure to the terrestrial radiation.

Acknowledgments We would like to thank Mr. Battsatsralt who served as the driver for the car-borne survey undertaken in the present study, and Ms. Ikeda, for drawing the figures presented in the present paper. We would also like to thank Dr. Sahoo (National Institutes for Quantum and Radiological Science and Technology, Japan) for fruitful discussions on radionuclide migration in the environment. This paper was improved by valuable and constructive comments from reviewers.

Funding information This work was supported by Fukushima Medical University (KKI29080 to Y.O.) and the Toyota Foundation (D16-R-0238 to C.Y.).

Compliance with ethical standards

Conflict of interest The authors declare that they have no conflicts of interest.

References

- Akata N, Ikeda T, Minato S, Shiroma Y, Shimo M (2017) A survey of a high natural radiation spot in Tono area, Japan. *Radiat Environ Med* 6:34–38
- Amante C, Eakins BW (2009) ETOPO1 1 arc-minute global relief model: procedures, data sources and analysis. NOAA Technical Memorandum NESDIS NGDC-24, National Geophysical Data Center, NOAA, Boulder. <https://doi.org/10.7289/V5C8276M>
- Ariunbileg S, Gaskova O, Vladimirov A, Battushig A, Moroz E (2016) Spatial distribution of uranium and metalloids in groundwater near sandstone-type uranium deposits, Southern Mongolia. *Geochem J* 50:393–401. <https://doi.org/10.2343/geochemj.2.0434>
- Baeza A, Corbacho JA, Miranda J (2013) Design and implementation of a mobile radiological emergency unit integrated in a radiation monitoring network. *IEEE Trans Nucl Sci* 60:1400–1407. <https://doi.org/10.1109/TNS.2013.2245511>
- Beamish D (2014) Environmental radioactivity in the UK: the airborne geophysical view of dose rate estimates. *J Environ Radioact* 138: 249–263. <https://doi.org/10.1016/j.jenvrad.2014.08.025>
- Bollhöfer A, Beraldo A, Pfitzner K, Esparon A, Doering C (2014) Determining a pre-mining radiological baseline from historic airborne gamma surveys: a case study. *Sci Total Environ* 468–469: 764–773. <https://doi.org/10.1016/j.scitotenv.2013.09.001>
- Boulestex T, Cathelineau M, Deloule E, Brouand M, Toubon H, Lach P, Fiet N (2019) Ilmenites and their alteration products, sinkholes for uranium and radium in roll-front deposits after the example of South Tortkuduk (Kazakhstan). *J Geochem Explor* 206:106343. <https://doi.org/10.1016/j.gexplo.2019.106343>
- Cardon O, Le Goux F, Salabert J (2015) Prospection d'uranium en Mongolie: découverte majeure dans le désert de Gobi. *Revue Générale Nucléaire* 47:12–19 (in French). <https://doi.org/10.1051/rgn/20156012>
- Dowdall M, O'Dea J (2002) $^{226}\text{Ra}/^{238}\text{U}$ disequilibrium in and upland organic soil exhibiting elevated natural radioactivity. *J Environ Radioact* 59:91–104. [https://doi.org/10.1016/S0265-931X\(01\)00038-8](https://doi.org/10.1016/S0265-931X(01)00038-8)
- Graham SA, Hendrix MS, Johnson CL, Badamgrav D, Badarch G, Amory J, Porter M, Barsbold R, Webb LE, Hacker BR (2001) Sedimentary record and tectonic implications of Mesozoic rifting in southeast Mongolia. *Geol Soc Am Bull* 113:1560–1579. [https://doi.org/10.1130/0016-7606\(2001\)113%3C1560:SRATIO%3E2.0.CO;2](https://doi.org/10.1130/0016-7606(2001)113%3C1560:SRATIO%3E2.0.CO;2)
- Greeman DJ, Rose AW, Washington JW, Dobos RR, Ciolkosz EJ (1999) Geochemistry of radium in soils of the Eastern United States. *Appl Geochem* 14:365–385. [https://doi.org/10.1016/S0883-2927\(98\)00059-6](https://doi.org/10.1016/S0883-2927(98)00059-6)
- Grizard P, Schmitt J-M, Goblet P (2019) Hydrogeology of an arid endorheic basin (Tsgaan Els, Dornogobi, Mongolia): field data and conceptualization, three-dimensional groundwater modeling, and water budget. *Hydrogeol J* 27:145–160. <https://doi.org/10.1007/s10040-018-1868-1>
- Hosoda M, Tokonami S, Omori Y, Sahoo SK, Akiba S, Sorimachi A, Ishikawa T, Nair RR, Jayalekshmi PA, Sebastian P, Iwaoka K, Akata N, Kudo H (2015) Estimation of external dose by car-borne survey in Kerala, India. *PLoS One* 10:e0124433. <https://doi.org/10.1371/journal.pone.0124433>
- Hosoda M, Inoue K, Oka M, Omori Y, Iwaoka K, Tokonami S (2016) Environmental radiation monitoring and external dose estimation in Aomori Prefecture after the Fukushima Daiichi Nuclear Power Plant accident. *Jpn J Health Phys* 51:41–50. <https://doi.org/10.5453/jhps.51.41>
- International Atomic Energy Agency (2018) World distribution of uranium deposit (UDEPO), 2016 edn. International Atomic Energy Agency, Vienna
- International Commission on Radiological Protection (2007) The 2007 recommendations of the International Commission on Radiological Protection. ICRP publication 103. *Annals of the ICRP* 37 (2–4). Elsevier, Amsterdam
- International Commission on Radiological Protection (2010) Conversion coefficients for radiological protection quantities for external radiation exposure. ICRP publication 116. *Annals of the ICRP* 40 (2–5). Elsevier, Amsterdam
- Le TV, Inoue K, Tsuruoka H, Fujisawa M, Arai M, Nguyen LDH, Somboon S, Fukushi M (2018) Effective dose due to terrestrial gamma radiation estimated in southern Vietnam by car-borne survey technique. *Radiat Prot Dosim* 179:18–25. <https://doi.org/10.1093/rpd/ncx185>
- Le Goux F, Banzragch T-O, Delaunay A, Nyamdorj B-I, Jaques E, Korshunov A, Parize O, Brouand M (2015) The major Gobi uranium deposits, upper Cretaceous East Gobi Basin, Mongolia: geodynamical and mineralogical key parameters of uranium ore geology. In: André-Meyer A-S, Cathelineau M, Muchez P, Pirard E, Sindre S (eds) Mineral resources in a sustainable world (proceedings of the 13th biennial SGA meeting 2015, Nancy, France, volume 5). The Society for Geology Applied to Mineral Deposits, Genève, pp 1815–1818

- Levinson AA, Bland CJ (1978) Examples of the variability of disequilibrium and the emanation factor in some uraniferous materials. *Can J Earth Sci* 15:1867–1871. <https://doi.org/10.1139/e78-194>
- Mangeret A, Blanchart P, Alcalde G, Amet X, Gazala C, Gallerand M-O (2018) An evidence of chemically and physically mediated migration of ^{238}U and its daughter isotopes in the vicinity of a former uranium mine. *J Environ Radioact* 195:67–71. <https://doi.org/10.1016/j.jenvrad.2018.08.018>
- Matsuda H, Minato S, Pasquale V (2002) Evaluation of accuracy of response matrix method for environmental gamma ray analysis. *Radioisotopes* 51:42–50 (in Japanese). <https://doi.org/10.3769/radioisotopes.51.42>
- Minato S (1978) A response matrix of a $3\phi \times 3$ NaI(Tl) scintillator for environmental gamma radiation analysis. *Rep Gov Ind Res Inst Nagoya* 27:384–397 (in Japanese with English abstract)
- Minato S (2001) Diagonal elements fitting technique to improve response matrixes for environmental gamma ray spectrum unfolding. *Radioisotopes* 50:463–471. https://doi.org/10.3769/radioisotopes.50.10_463
- Momčilović M, Kovačević J, Tanić M, Đorđević M, Bačić G, Dragović S (2013) Distribution of natural radionuclides in surface soils in the vicinity of abandoned uranium mines in Serbia. *Environ Monit Assess* 185:1319–1329. <https://doi.org/10.1007/s10661-012-2634-9>
- Morishima H, Koga T, Tatsumi K, Nakai S, Sugahara T, Yuan Y, Wei L (2000) Dose measurement, its distribution and individual external dose assessments of inhabitants in the high background radiation areas in China. *J Radiat Res* 41:S9–S23. <https://doi.org/10.1269/jrr.41.S9>
- Nair RRK, Rajan B, Akiba S, Jayalekshmi P, Nair MK, Gangadharan P, Koga T, Morishima H, Nakamura S, Sugahara T (2009) Background radiation and cancer incidence in Kerala, India–Karunagappally cohort study. *Health Phys* 96:55–66. <https://doi.org/10.1097/01.HP.0000327646.54923.11>
- Nriagu J, Johnson J, Samurkas C, Erdenechimeg E, Ochir C, Chandaga O (2013) Co-occurrence of high levels of uranium, arsenic, and molybdenum in groundwater of Dornogobi, Mongolia. *Glob Health Perspect* 1:45–54. <https://doi.org/10.5645/ghp2013.01.01.07>
- Omori Y, Sorimachi A, Gun-Aajav M, Enkhgerel N, Oyunbolor G, Palam E, Yamada C (2019) Elevation of gamma dose rate by construction of the Asian Highway 3 (AH3) between Ulaanbaatar and Sainshand, Mongolia. *Radiat Prot Dosim* 184:127–134. <https://doi.org/10.1093/rpd/ncy173>
- Prost GL (2004) Tectonics and hydrocarbon systems of the East Gobi basin, Mongolia. *AAPG Bull* 88:483–513. <https://doi.org/10.1306/11150303042>
- Quindós LS, Fernández PL, Soto J, Ródenas C, Gómez J (1994) Natural radioactivity in Spanish soils. *Health Phys* 66:194–200. <https://doi.org/10.1097/00004032-199402000-00010>
- Saleh MA, Ramli AT, Hamzah KB, Alajerami Y, Moharib M, Saeed I (2015) Prediction of terrestrial gamma dose rate based on geological formations and soil types in the Johor State, Malaysia. *J Environ Radioact* 148:111–122. <https://doi.org/10.1016/j.jenvrad.2015.05.019>
- Kocher DC, Sjoreen AL (1985) Dose-rate conversion factors for external exposure to photon emitters in soil. *Health Phys* 48:193–205. <https://doi.org/10.1097/00004032-198502000-00006>
- Tao Z, Akiba S, Zha Y, Sun Q, Zou J, Li J, Liu Y, Yuan Y, Tokonami S, Morishima H, Koga T, Nakamura S, Sugahara T, Wei L (2012) Cancer and non-cancer mortality among inhabitants in the high background radiation area of Yangjiang, China (1979–1998). *Health Phys* 102:173–181. <https://doi.org/10.1097/HP.0b013e31822c7f1e>
- Torres SB, Petrik A, Szabó KZ, Jordan G, Yao J, Szabó C (2018) Spatial relationship between the field-measured ambient gamma dose equivalent rate and geological conditions in a granite area, Velence Hills, Hungary: an application of digital spatial analysis methods. *J Environ Radioact* 192:267–278. <https://doi.org/10.1016/j.jenvrad.2018.07.001>
- Tserenpil S, Maslov OD, Norov N, Liu QC, Fillipov MF, Theng BKG, Belov AG (2013) Chemical and mineralogical composition of the Mongolian rural soils and their uranium sorption behavior. *J Environ Radioact* 118:105–112. <https://doi.org/10.1016/j.jenvrad.2012.11.016>
- United Nations Scientific Committee on the Effects of Atomic Radiation (2010) Sources and effects of ionizing radiation, UNSCEAR 2008 report to the general assembly with scientific annexes, volume I. United Nations, New York
- Yamada C, Tsendendamba B, Horiuchi T, Katagiri K, Suenaga K, Palam E (2018) Introduction of a community initiative activity preparing to respond to radiation exposure in Mongolia: a research prior to the intervention. *J Jpn Soc Int Nurs* 1:25–34 (in Japanese with English abstract)
- Yoshioka Y (1994) Study of time variation of terrestrial gamma radiation due to depth distribution of soil moisture content. *Radioisotopes* 43:183–189. <https://doi.org/10.3769/radioisotopes.43.183>
- Vandenhove H, Sweeck L, Mallants D, Vanmarcke H, Aitkulov A, Sadyrov O, Savosin M, Tolongutov B, Mirzachev M, Clerc JJ, Quarch H, Aitaliev A (2006) Assessment of radiation exposure in the uranium mining and milling area of Mailuu Suu, Kyrgyzstan. *J Environ Radioact* 88:118–139. <https://doi.org/10.1016/j.jenvrad.2006.01.008>
- Vandenhove H, Verrezen F, Landa ER (2010) Radium. In: Atwood DA (ed) *Radionuclides in the environment*. John Wiley & Sons, Ltd., Chichester, pp 97–108
- Von Gunten HR, Surbeck H, Rössler E (1996) Uranium series disequilibrium and high thorium and radium enrichment in Karst formations. *Environ Sci Technol* 30:1268–1274. <https://doi.org/10.1021/es950473j>
- War SA, Nongkynrih P, Khathing DT, Iongwai PS, Jha SK (2008) Spatial distribution of natural radioactivity levels in topsoil around the high-uranium mineralization zone of Kylleng-Pyndensohiong (Mawthabang) areas, West Khasi Hills District, Meghalaya, India. *J Environ Radioact* 99:1665–1670. <https://doi.org/10.1016/j.jenvrad.2008.04.014>
- Wessel P, Smith WHF, Scharroo R, Luis J, Wobbe F (2013) Generic mapping tools: improved version released. *EOS Trans AGU* 94:409–410. <https://doi.org/10.1002/2013EO450001>

Publisher's note Springer Nature remains neutral with regard to jurisdictional claims in published maps and institutional affiliations.